

Discovery and Mechanistic Investigation of Photoinduced sp³ C–H activation of Hydrocarbons by the Simple Anion Hexachlorotitanate

Grace B. Panetti,^{1,2} Qiaomu Yang,¹ Michael R. Gau,¹ Patrick J. Carroll,¹ Patrick J. Walsh,*¹ and Eric J. Schelter*^{1,3}

¹Roy and Diana Vagelos Laboratories, Department of Chemistry, University of Pennsylvania 231 South 34th St. Philadelphia, PA 19104 (USA) ²Current affiliation: Department of Chemistry, Frick Laboratory, Princeton University, Princeton, NJ 08544, (USA) ³lead Contact

*Correspondence: pwalsh@sas.upenn.edu; schelter@sas.upenn.edu Lead Contact email: schelter@sas.upenn.edu

SUMMARY

The selective transformation of hydrocarbons into more chemically complex materials is an evergreen challenge in chemistry and catalysis. This report finds the dianion hexachlorotitanate ($TiCl_6^{2-}$) catalyzes the C–H activation of saturated hydrocarbons under 390 nm light irradiation. Investigations into the mechanism of this reaction are detailed. The photolysis event affords formation of a chlorine radical and a mixture of $Ti^{III}Cl_4(NCMe)_2^{-}$ and $Ti^{III}Cl_5(NCMe)_2^{-}$. The $Ti^{III}Cl_8$ species were characterized by spectrophotometry, electrochemistry, and X-ray crystallography. Alkyl radicals generated by these means were trapped by a range of alkene acceptors. Notably, the $Ti^{III}Cl_8$ species are shown to be more reducing ($\Delta E_{pa} = 0.72$ V) than related $Ce^{III}Cl_8$ species, enabling access to more electron-rich acceptors by facilitating reduction of the alkyl radical trapped intermediate. DFT calculations correctly identify the reactivity of alkene substrates using the $CeCl_6^{2-}$ and $TiCl_6^{2-}$ photoredox catalysts. The results herein demonstrate the impact of metal identity on C–H activation.

1



INTRODUCTION

Selective functionalization of alkane substrates has proven to be difficult as their C-H bonds have bond dissociation energies (BDE) as high as 105 kcal mol-1 in the gas phase.1 One of the earliest reported methods of functionalizing methane and other hydrocarbons was the use of radical species, notably chlorine radical (BDE of H–Cl $103~\rm kcal~mol^{-1}$). ^{2,3} The chlorination of methane has been performed using chlorine gas and ultraviolet light, a process which generates many industrially relevant chlorinated solvents.⁴ However, due to high concentrations of chlorine radicals generated, the use of chlorine gas is unselective and results in mixtures of $CH_{4-x}CI_x = 1 - 4$ species.⁵ Recent studies in C–H activation have used photocatalysis to produce catalytic amounts of chlorine radicals. Photoredox catalysis uses light to perform the oxidation of chloride anion to chlorine radical, estimated at +1.63 vs. Fc/Fc+,6 enabling control of the concentration of chlorine radicals and facilitating selective chemistry. 7-10 This approach has been developed using outer sphere charge transfer mechanisms with IrIII photoredox notably by Barriault and co-workers.¹¹ Alternatively, inner-sphere ligand to metal charge transfer (LMCT) mechanisms have been investigated by Doyle using Ni^{III}_CI species, ^{12,13} Rovis using Cu^{II}_CI species,¹⁴ and our groups and Zuo using Ce^{IV}–Cl species (Figure 1a).¹⁵⁻¹⁷ Additional recent reports from Rovis, Jin and Dual have also demonstrated the abilities of Fe^{III}Cl₃ species to engage in similar chemistry. 18-20 The realization that chlorine radicals can be easily generated under photochemical conditions through LMCT prompted us to consider alternative metal chloride species that could offer distinct benefits. Notably, the chemistry with alkene radical acceptors involves a formal H atom transfer event, which can be deconvoluted as proton transfer from acid and electron transfer from the reduced metal species. Our efforts were then focused on metal cations that would 1) enable a broader scope of radical acceptors and 2) employ abundant and less expensive metal sources. Based on these characteristics, we identified Ti^{IV} complexes as potentially suitable catalysts.

Prior catalytic photochemical reactions driven by titanium have been limited to solid phase titanium chromophores. ²¹⁻²³ Stochiometric photoreactivity of titanium species has been previously observed towards the production of Ti^{III} species and oxidized ligands. ²⁴⁻²⁶ More recently, the groups of Gansäuer and Flowers reported use of Cp₂TiCl₂ in a photoredox reaction to perform the ring opening of epoxides employing a weak amine sacrificial reductant (**Figure 1b**) avoiding the use of strong heterogenous reductants like Zn⁰ or Mn^{0,27,28} With this success, and the similarity of the available redox states between titanium and cerium, we hypothesized that the CeCle²⁻ mediated system described by Zuo, Schelter, and Walsh could be translated into an analogous TiCl₆²⁻ system with added benefits.

Figure 1. Photoredox reactions.

A. Examples of reported systems that used SET and LMCT transitions to generate chlorine radicals. B. Reported photocatalytic Ti^{IV} species. C. This work, which uses photolytic breaking of titanium chloride bonds to enable the C–H bond alkylation of unactivated hydrocarbons towards the hydroalkylation of electron poor alkenes.



A. Generation of CI radical species by photoactive species

B. Recent homogeneous Ti photocatalysis

C. This work

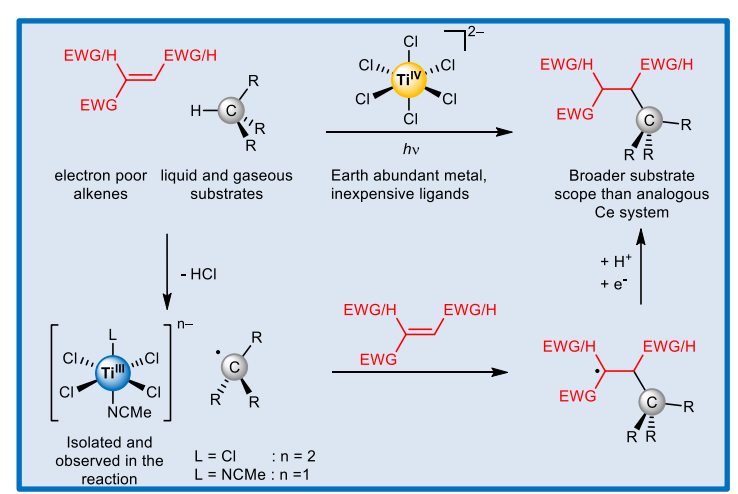


Figure 1. Photoredox reactions.

A. Examples of reported systems that used SET and LMCT transitions to generate chlorine radicals. B. Reported photocatalytic Ti^{IV} species. C. This work, which uses photolytic breaking of titanium chloride bonds to enable the C–H bond alkylation of unactivated hydrocarbons towards the hydroalkylation of electron poor alkenes.

Herein, we report the use of the simple titanium chloride salt $[PPh_4]_2[TiCl_6]$ in the photolytic cleavage of C–H bonds in hydrocarbon substrates. Hydrocarbons, including methane, are functionalized through hydrogen atom transfer processes (**Figure 1 c**). We demonstrate that the substrate scope of radical acceptors is broader using $TiCl_6^2$ compared to the cerium based $(CeCl_6^2)$ system. The expanded scope of the titanium system is rationalized through comparison of the redox potentials of the $Ce^{||C|_{x}}$ and $Ti^{||C|_{x}}$ intermediates, where the $Ti^{||C|_{x}}$ species are more strongly reducing. Relevant $Ti^{||C|_{x}}$ species were isolated and identified by X-ray crystallography, as well as observed in the reaction media using UV-vis spectroscopy. The excited state of the photocatalyst was interrogated by TD-DFT and the reaction coordinate was modeled using DFT. The findings support the hypothesis that the reduction of the radical intermediate is integral to formation of the product of alkyl radical trapping.



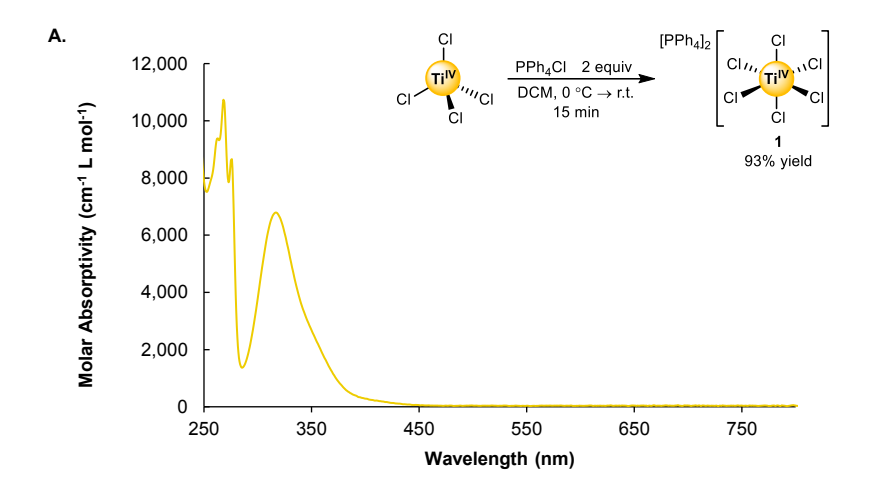
RESULTS

Initial discovery of TiCl₆2⁻ photolytic sp³ C-H activation

Based on the recent implementation of the cerium photoredox catalyst CeCl₆²⁻, and similarities in electronic states between Ce^{IV} and Ti^{IV} , we envisioned the use of $TiCl_6^{2-}$ as a starting point for new catalyst discovery. The TiCl₆²⁻ dianion was selected because a homoleptic complex was expected to provide the most straightforward electronic states and spectroscopic signature, and would be the least likely to undergo ligand decomposition. The complex [PPh₄]₂[TiCl₆] (1) was easily synthesized from commercially available precursors TiCl₄ and PPh₄Cl (Figure 2a), which reduced the number of synthetic steps and increased the yield compared to the previous method using $[NH_4]_2[TiF_6]$. The resulting complex was easily recrystallized from acetonitrile and obtained in 93% yield. Compound 1 was significantly more stable toward air and water than TiCl₄, as TiCl₄ fumes upon exposure to air, while solutions of ${f 1}$ in acetonitrile do not fume and were stable for hours under air. The UV-Vis of ${f 1}$ revealed a single peak at wavelengths higher than 300 nm, centered at 318 nm. This broad peak shows trailing intensity into the visible region, resulting in the compound's yellow color. Expecting that this absorption would comprise $Cl^- \to Ti^{IV}$ LMCT character similar to the $CeCl_6^{2^-}$ anion, 30 we investigated the ability of [PPh₄]₂[TiCl₆] to activate C–H bonds through the formation of Cl radicals.

Toluene (2a) was chosen as a model substrate due to its relatively weak benzylic C–H bonds ($89.7~\rm kcal~mol^{-1}$). Irradiation of a suspension of [PPh4]2[TiCl6] in acetonitrile (MeCN) with 10 equiv toluene using a light source centered at 390 nm (containing light between 370 nm and 420 nm, see SI for details) over 22 h resulted in a pale blue solution (**Figure 2b**). UV-Vis analysis revealed a new transition at $685~\rm nm$, which accounted for the blue color. Exposing this solution to air regenerated the yellow solution of $TiCl_6^{2-}$ with disappearance of the peak at $685~\rm nm$. Performing this same reaction in an air-free NMR tube in MeCN- d_3 solvent afforded detection of benzyl chloride (2a-Cl) and bibenzyl ($2a_2$) as the organic products of the reaction in a $1:3~\rm ratio$. The appearance of these products indicated that, upon photoirradiation, toluene underwent HAT to generate a benzyl radical. The benzylic radical gave rise to the dimerization product, bibenzyl, and benzyl chloride, presumably by reaction with Cl⁻. We rationalized that the blue color of the solution was likely a Ti^{III} species based on 1) its formation upon oxidation of toluene and 2) its sensitivity to air. The nature of this Ti^{III} species is discussed further below. Having demonstrated that $TiCl_6^{2-}$ is capable of activating sp³ C–H bonds, we next focused on determining if $TiCl_6^{2-}$ could perform alkane functionalizations under catalytic conditions.





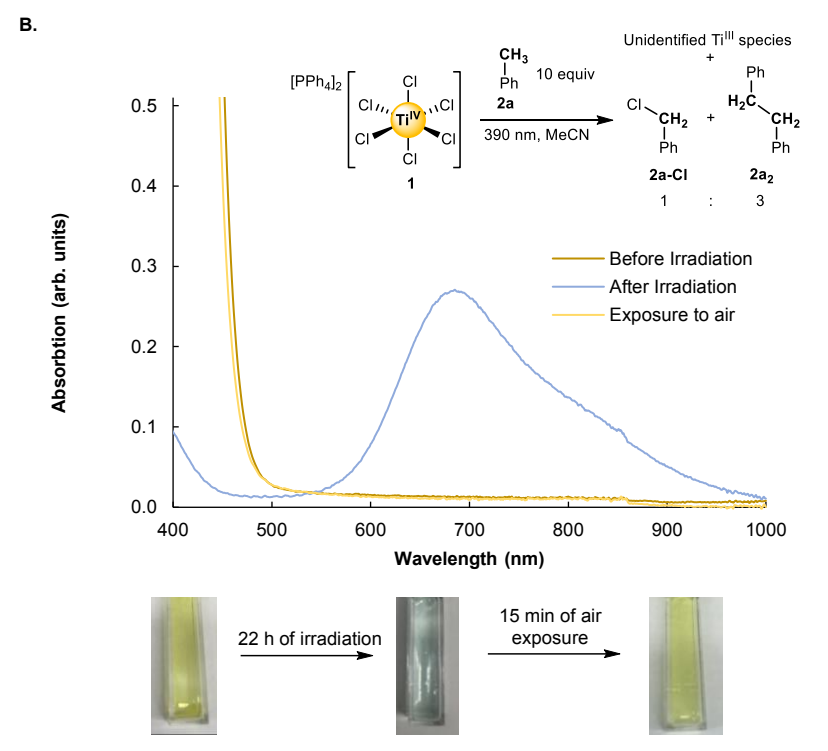


Figure 2 Initial discovery of $TiCl_6^{2-}$ photoreactivity

A. Synthesis and UV-Vis spectra of $[PPh_a]_2[TiCl_6]$ in MeCN 1. B. Photolysis experiments of 1 with 2a with the identity of the organic products, benzyl chloride (2a-Cl) and bibenzyl ($2a_2$), produced in a 1 : 3 ratio. The UV-Vis analysis of this reaction is additionally shown. Pictures of the air-free cuvette during this analysis are provided.

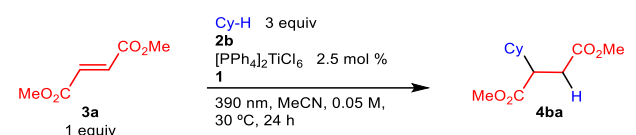
TiCl₆²⁻ as a photoinduced C-H activation catalyst

For the catalytic studies we chose to use $[PPh_4]_2[TiCl_6]$ with a prototypical alkane substrate, cyclohexane (BDE C–H: 100 kcal mol⁻¹; **2b**). Using 2.5 mol% $[PPh_4]_2[TiCl_6]$ with an excess of cyclohexane (3 equiv), dimethyl fumarate (3a) as the radical acceptor, and 24 h irradiation at rt, an 88% AY (AY = assay yield, as determined by integration of the product ¹H NMR against an internal standard) of the hydroalkylated alkene was obtained (**Table 1**, entry 1). Conducting the reaction in the absence of light resulted in no observable product and recovery of most of 3a (**Table 1**, entry 2). Attempts to thermally promote the reaction by heating the catalyst and coupling partners to 80 °C did not generate any detectable product but resulted in near complete recovery of 3a (**Table 1**, entry 3). Replacing the 390 nm light with a



longer wavelength of light (467 nm) did not form product nor result in consumption of starting material (88% recovery of 3a, Table 1, entry 4). Additionally, replacing the 390 nm light with a shorter wavelength of light (370 nm) resulted in reduced amounts of 4ba produced (Table \$1). Attempting the reaction without $[PPh_4]_2[TiCl_6]$ or replacing the $[PPh_4]_2[TiCl_6]$ with [PPh4]2[CeCl6] resulted in no product. The catalyst free conditions resulted in near complete recovery of 3a (91%, entry 5). In the case of the cerium catalyst a small amount of 3a was consumed (68% recovery of 3a, entry 6). When optimizing the reaction, increasing the molarity of the reaction or decreasing the amount of cyclohexane resulted in a lower reaction yield. Use of acetone in place of acetonitrile resulted in a significant decrease in yield, while using DMF completely halted the reaction (Table S1). A light on/light off experiment provided evidence that constant irradiation from the 390 nm light was necessary for formation of the product (Figure \$10). With the optimized reaction conditions (Table 1, entry 1), we proceeded to To investigate the investigate the scope of the hydrocarbon and radical acceptors. scope of liquid alkanes, we focused on a series of cyclic hydrocarbons (Figure 3). Cyclohexane (2b), cycloheptane (2c), and cyclooctane (2d) all react similarly with 3a resulting in 74% 4ba, 74% 4ca, and 79% 4da isolated yields, respectively. Using three equiv cyclopentane (2e) resulted in incomplete conversion of 3a to the hydroalkylated product (4ea). Increasing the amount of cyclopentane to 4.5 equiv resulted in complete consumption of 3a and an isolated yield of 84% of the addition product 4ea.

Table 1. Control reactions of the photolytic C-H activation of cyclohexane with [PPh₄]₂[TiCl₆].



Entry	Deviation	4ba (%)	3a (%)
1	None	88 (74)	6
2	No light	0	90
3	No light 80 °C	0	94
4	Use 467 nm light instead of 390 nm	0	88
5	No 1	0	91
6	Use [PPh ₄] ₂ [CeCl ₆] instead of 1	0	68

Standard reaction conditions: 0.2 mmol of 3a, 0.6 mmol of cyclohexane 2b, 0.005 mmol of $[PPh_4]_2[TiCl_6]$ 1 in 4 mL of MeCN irradiated by 390 nm light. Assay yields were determined by 1H NMR integration of the crude reaction mixture as compared to 0.1 mmol of CH_2Br_2 internal standard added after the reaction. Values in parentheses are isolated yields.

The scope of the radical acceptors was examined next. We found a comparatively large scope of electron-deficient alkenes were hydroalkylated under the reaction conditions compared to reactions using CeCle²⁻. The reaction was also viable with alkenes bearing nitriles, sulfones, and imides. With N-phenyl maleimide (3e) as the radical trap, significant amounts of side products were observed and the desired adduct 4be was obtained in 43% yield. This result could be due, in part, to the known photo reactivity of malimides. The reactions using methyl atropate (3d) and benzylidene malononitrile (3g) (products 4bd and 4bg) were not completely consumed under the standard conditions. Using either a higher loading of catalyst (5 mol% for 4bd) or a longer reaction time (48 h for 4bg) resulted in complete consumption of the alkene with isolated yields of 63% and 86%, respectively. Using dimethyl 2-(trichloromethyl)fumarate (3h) with cyclohexane resulted in chloride elimination and the formation of a dichloromethylene containing product 4bh in 30% yield. Limitations of the scope are outlined in Figure S4.

While liquid hydrocarbons had proven to be suitable substrates, it was unknown if [PPh₄]₂[TiCl₆] (1) could activate gaseous hydrocarbons. Such reactions are inherently more difficult due to the higher BDE's and lower solubility of light hydrocarbons in polar solvents like acetonitrile. Under an atmospheric pressure of ethane (2f) and using 5 mol% of 1, hydroalkylated products with radical acceptors 3c or 3g resulted in 50% and 71% isolated yields, respectively. We found that while 3g was successful at accepting ethane radicals, longer reaction times were necessary for the complete consumption of 3g. Methane (2g), due to its lower solubility and reduced reactivity, required a pressure of 50 atm for reasonable conversion. Due to the difficulty associated with using methane additional optimization was required. We found that decreasing the concentration of radical acceptor from 0.05~M to 0.01~MM, and using a combination of 10 mol % TiCl4(MeCN)2 MeCN and 20 mol % PyrHCl as the source of the TiCl₆²⁻ anion for methane conversion. However, isolation of methylated product 4gc by chromatography proved to be challenging due to its similarities with the hydrogenated alkene byproduct. We hypothesized that the hydrogenation results from protons derived from the HCl generated in the reaction media and electrons originating from Ti^{III} species in solution. However, the isolation of the product 4gg via column chromatography proved to be much easier,



despite the presence of hydrogenated species. With the scope of the reaction outlined, we shifted our attention to the mechanism of the reaction.

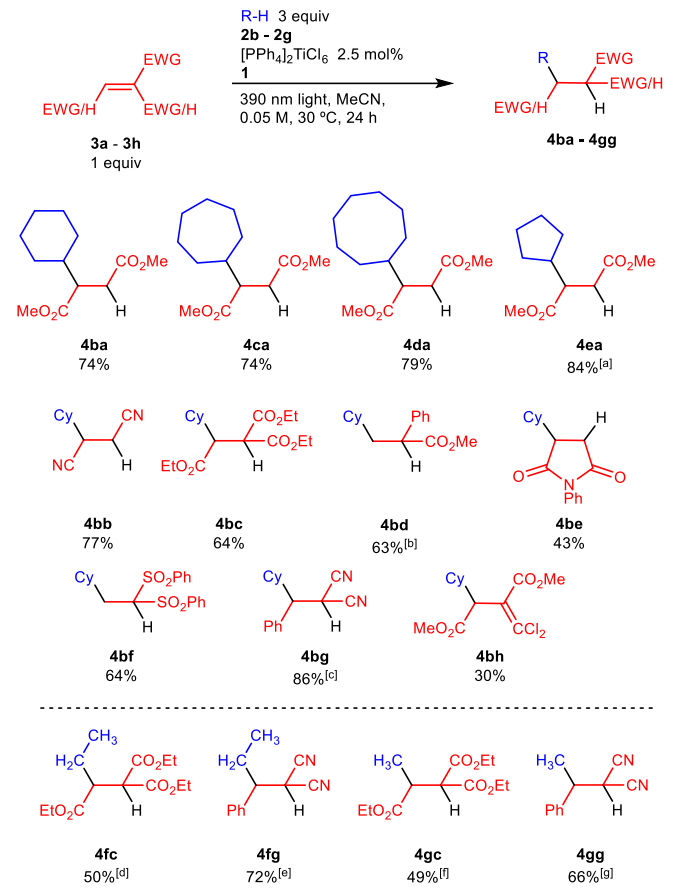


Figure 3. Substrate scope of the $[PPh_4]_2[TiCl_6]$ mediated hydroalkylation of electron deficient alkenes. $^{[n]}$ 4.5 equiv of alkane. $^{[n]}$ 5 mol $^{(n)}$ of $[PPh_4]_2[TiCl_6]$. $^{[n]}$ 48 h. $^{(n)}$ 1 atm of ethane, 5 mol $^{(n)}$ of $[PPh_4]_2[TiCl_6]$, 48 h. $^{(n)}$ 50 atm of methane, 10 mol $^{(n)}$ of $TiCl_4(MeCN)_2$ -MeCN, 20 mol $^{(n)}$ PyrHCl, 0.01M, Yield determined by $^{(n)}$ HNMR integration vs an CH₂Br₂ internal standard. $^{(n)}$ 50 atm of methane, 10 mol $^{(n)}$ of $TiCl_4(MeCN)_2$ -MeCN, 20 mol $^{(n)}$ PyrHCl, 0.01 M, 48 h.

Investigation of the selectivity of the reaction

To identify the species responsible for the C–H activation, the reactivity of [PPh4]2[TiCl₆] (1) with n-pentane and 2,3-dimethyl butane, which contain 1° and 2°, and 1° and 3° C–H bonds, respectively was investigated. Of the alkenes employed in the investigation of catalysis, the 1,1-disulfonyl alkene **3f** was chosen due to its reduced steric effects during C–C bond formation. The reaction with n-pentane gave a 1° to 2° selectivity activation ratio of 28: 72 (**Figure S5-7**). The reaction with 2,3-dimethyl butane gave a selectivity of 42: 58 for activation at the 1° versus 3° C–H bonds. These selectivity ratios are consistent with reported values for Cl⁻ radicals in acetonitrile. 15 Based on the similarities of C–H HAT selectivities with those known for Cl⁻ and the formation of benzyl chloride and bibenzyl upon reaction with toluene (**Figure 2b**), we propose that Cl⁻ is generated upon irradiation of TiCl₆2⁻. Upon dissociation of Cl⁻, a blue intermediate, presumably Ti^{III}, was formed. We next investigated possible Ti^{III} intermediates in this process.

Investigation of the Ti^{III} species present in the reaction

The reduced form of the catalyst plays an important role in product formation and catalyst turnover. To test our hypothesis that the $Ti^{III}CI_x$ species in solution would be more reducing than the related $Ce^{III}CI_x$ species, we turned to electrochemical analysis. Cyclic voltammetry of $[PPh_4]_2[TiCI_6]$ (1) in MeCN using NEt₄CI as the electrolyte revealed a quasi-reversible wave with



 $E_{pc} = -0.99$ V and $E_{pa} = -0.68$ V versus Fc/Fc⁺ (**Figure 4a**). This cathodic potential is significantly more reducing than the analogous conditions with CeClo²⁻; CeClo²⁻ has a reversible wave centered at $E_{1/2} = +0.03$ V vs Fc/Fc⁺ (**Figure 4a**).³⁰ The observed redox potentials support our hypothesis that Ti^{III}Cl_x species are more reducing than Ce^{III}Cl_x species under identical conditions. This observation allows the TiClo²⁻ catalyzed system to more easily reduce the radical-based intermediates formed from radical addition to electron poor alkenes, thereby enabling TiClo²⁻ catalysis to have a broader radical acceptor scope than CeClo²⁻ mediated catalysis. We then turned our attention to spectroscopic observation, isolation and characterization of the Ti^{III}Cl_x intermediate.

To investigate the identity of the blue species observed in the stoichiometric reactivity studies (Figure 2b), we monitored Ti^{III} speciation in the presence of varying amounts of chloride in acetonitrile by electronic absorption spectroscopy (Figure 4b). Using the Ti^{III} starting material $TiCl_3(THF)_3^{34}$ dissolved in MeCN, we titrated the titanium complex with [nBu_4N]Cl to investigate its speciation. Structural studies to determine (Ti^{III}Cl_x)n- species in weakly coordinating solvents including DCM have been previously investigated, resulting in multimetallic species with bridging chlorides.^{35,36} We expected these studies were not relevant to our catalytic system, as the strongly coordinating acetonitrile will likely cause different behavior. Addition of the first equiv of chloride to TiCl₃(THF)₃ resulted in a color change from purple ($\lambda_{max} = 589$ nm) to blue (λ_{max} = 685 nm) with an isosbestic point at 634 nm (**Figure S13**). The two species from this set of data were expected to be the Ti^{III}Cl₃(NCMe)₃ and Ti^{III}Cl₄(NCMe)₂. Continuing the titration to 30 equiv Cl⁻ produced a green solution, with a new peak growing in at $(\lambda_{max} = 430 \text{ nm})$ over the course of the titration, and an isosbestic point was observed at 607 nm. We expected the relevant species over these concentrations of chloride to be Ti^{III}Cl₄(NCMe)₂- and Ti^{III}Cl₅(NCMe)²-. The observed isosbestic point allowed the quantification of the equilibrium constant of the two species identified as $K_{eq} \approx 0.88$ using the intensities of the peaks at 685 nm and 430 nm. We then set out to isolate relevant $Ti^{\parallel}Cl_x$ species and characterize them by X-ray crystallography.

Treating TiCl₃(THF)₃ with 1.33 equiv of PPh₄Cl in acetonitrile resulted in the isolation of blue crystals (76% yield) that were identified as trans-[PPh₄][TiCl₄(MeCN)₂] (**Figure 4c, 5a**). Increasing to 5 equiv of PPh₄Cl resulted in a green solution that, upon diethyl ether vapor diffusion, produced yellow crystals (80% isolated yield), which were identified as [PPh₄]₂[TiCl₅(MeCN)] (**5b**). Both complexes have longer Ti-Cl bonds than the reported distances for the TiCl₆²⁻ (Ti–Cl average bond distance: 2.342 Å).²⁹ These observations strongly support a Ti^{III} oxidation state.

Measuring the solution UV-Vis spectra of the catalytic C–H functionalization with dimethyl fumarate revealed a peak of increasing intensity centered at 685 nm. This peak matched the signal observed in the stoichiometric C–H activation study, the UV-Vis titration, and corresponds to trans-[PPh₄][TiCl₄(MeCN)₂] (**5a, Figure 4d**). The concentration of trans-[PPh₄][TiCl₄(MeCN)₂] increased over the course of the reaction from 1.1 mM after 1 h to 2.1 mM after 5 h. These timepoints account for 51% to 84%, respectively, of the Ti species present in the reaction mixture (total 2.5 mM). Having established the probable speciation of the catalyst, computation was used to probe the working mechanistic hypothesis.



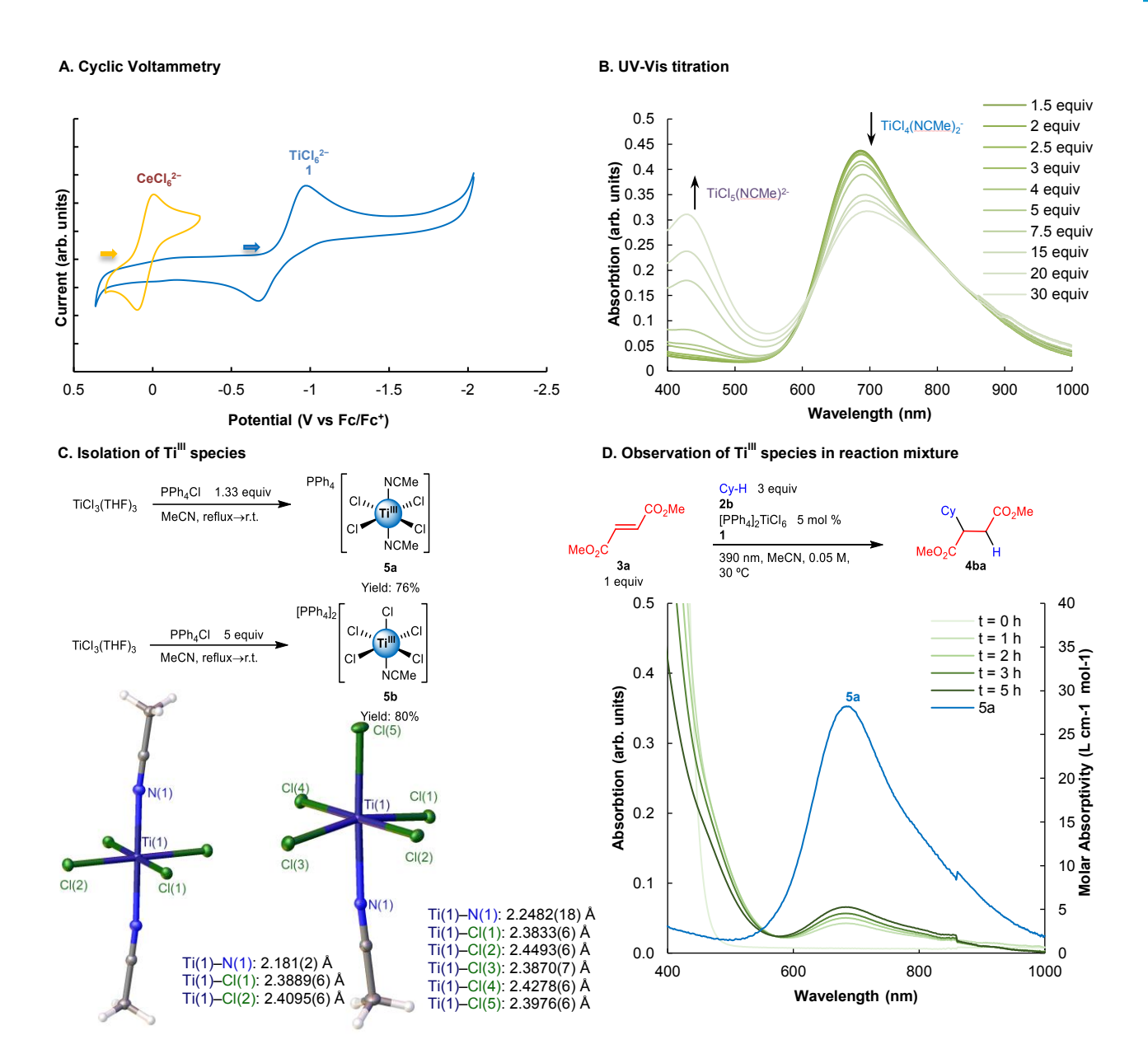


Figure 4. Determination of Ti^{III} species

A. Cyclic voltammetry of [PPh4]2[TiCla] (blue) and [PPh4]2[CeCla] (orange). Solvent = MeCN, $\nu=100$ mVs⁻¹, [Sub] = 0.001 M, [Et4N]Cl = 0.1 M. **B.** UV-Vis titration of TiCl3(THF)3 with [^Bu4N]Cl in MeCN. The reduction of the peak at 635 nm corresponds to TiCl4(MeCN)2⁻ and the growth of a peak centered at 430 nm corresponds to TiCl5(MeCN)2⁻. Keq = 0.88. **C.** The syntheses and thermal ellipsoid plots of **5a** and **5b** at the 30% confidence level with selected bond lengths. Cations and interstitial solvent removed for clarity. **D.** Monitoring the catalytic C–H functionalization via UV-Vis spectroscopy and comparison of the visible light portion of the spectra with the UV-Vis spectrum of **5a**.

Computational assessment

Computational studies were initiated using the M06-2X functional and Dunning's correlation consistent triple zeta basis sets with diffuse function augmentation to evaluate the reaction path.^{37,38} First, we calculated the energy of the vertical excitation corresponding to the absorption of light in [PPh4]2[TiCl6] (1). We determined that, in an octahedral geometry, the first vertical excitation with significant oscillator strength is an excitation from the t_{10} HOMO-1 orbital (comprising 3 % Ti character and 97 % CI character) into the t_{2g} LUMO orbital (comprising 84 % Ti character and 16 % CI character; **Figure \$52**). The energy of the associated primarily



LMCT band is at 297 nm (4.17 eV; 96.3 kcal mol⁻¹) and matches well with the experimentally determined λ_{max} of TiCl₆²⁻ at 318 nm (3.90 eV; 89.9 kcal mol⁻¹). This energy difference is quite small and often observed in TD-DFT calculations.³⁹ Additionally, calculations of the first singlet vertical excitation and lowest triplet state are 83.4 kcal mol⁻¹ and 48.7 kcal mol⁻¹ higher respectively than the ground state singlet of TiCl₆²⁻. The relevant absorption band, first singlet excited state, and triplet state are all higher in energy than the sum of Ti^{III}Cl₅(MeCN)⁻ + Cl⁻¹ (39.4 kcal mol⁻¹ higher than ground state TiCl₆²⁻ and MeCN). The relative energy differences indicated that these excited states may be species along a pathway of chlorine radical elimination. Following our investigation into the excited state species, we focused on a probable mechanism of the reaction.

We followed the general mechanism for photocatalytic C–H activation as a starting point to study the reaction mechanism computationally (**Figure S48**). First, there is the photoexcitation of $Ti^{IV}Cl_6^{2-}$ (**I**) into its excited state (ES). Upon vibronic relaxation, this excited state generates $Ti^{III}Cl_5(MeCN)^{2-}$ and ${}^{\bullet}Cl$ (**II**). CI radical promotes the HAT from the C–H bond of the hydrocarbon substrate (**TS I**) to produce HCl and a carbon-centered radical (**III**). Here the radical can be intercepted by the electron poor alkene through radical addition (**TS II**) to generate a new radical species (**IV**). Radical **IV** is then reduced by Ti^{III} . It is noteworthy that $Ti^{III}Cl_5(MeCN)^{2-}$ is in equilibrium with $Ti^{III}Cl_4(MeCN)^{2-}$ and chloride; however, we expect that $Ti^{III}Cl_5(MeCN)^{2-}$ is a superior reductant. Thus, $Ti^{III}Cl_5(MeCN)^{2-}$ reduces the radical to generate an anionic organic species and $Ti^{IV}Cl_5(MeCN)^-$ (**V**). The organic anion is protonated by HCl to generate product (**VI**) and the remaining chloride is intercepted by $Ti^{IV}Cl_5(MeCN)^-$ regenerating $Ti^{IV}Cl_5(^{2-}$ (**VII**). With this probable mechanism established computationally, we examined the energy profile of different hydrocarbon substrates and electron deficient alkenes.

We investigated the impact of the radical acceptor using a model isopropyl radical. We examined three groups of alkene substrates. The first is an alkene substrate that did not produce the radical addition products with either $CeCl_6^2$ - or $TiCl_6^2$ -; methyl cinnamate, **3i.** Next were a pair of substrates that perform well with $Ti^{IV}Cl_6^2$ - but were not viable using $Ce^{IV}Cl_6^2$ -: dimethyl fumarate and methyl atropate, **3a** and **3d.** Lastly, trimethyl ethylenetricarboxylate, **3i**, in which products with both $Ce^{IV}Cl_6^2$ - or $Ti^{IV}Cl_6^2$ - were formed (**Figure 5**). We observed the peaks of the energy landscape following the excited state (**TS II**) and intermediate (**V**), there are three groups of energy regimes which correspond to the three previously stated alkene categories. The highest energy state being the formation of the methyl cinnamate anion from $Ti^{III}Cl_5(MeCN)^2$ - ($\Delta G = 50.4$ kcal mol-1, intermediate **V**). With the substrates that perform with $TiCl_6^2$ - but not $CeCl_6^2$ - the reduction event occurs at $\Delta G = 39.4 - 40.6$ kcal mol-1, and triethyl ethenetricarboxylate based reduction occurs at $\Delta G = 23.2$ kcal mol-1. This observation agrees with our hypothesis that the ability of the catalyst to turn over the substrate is dependent on its ability to reduce the radical intermediate to the anion.

Figure 5. Energy profile of the catalytic reaction.

Radical traps: methyl cinnamate 3i, 3a, 3d, and trimethyl ethylenetricarboxylate 3j.



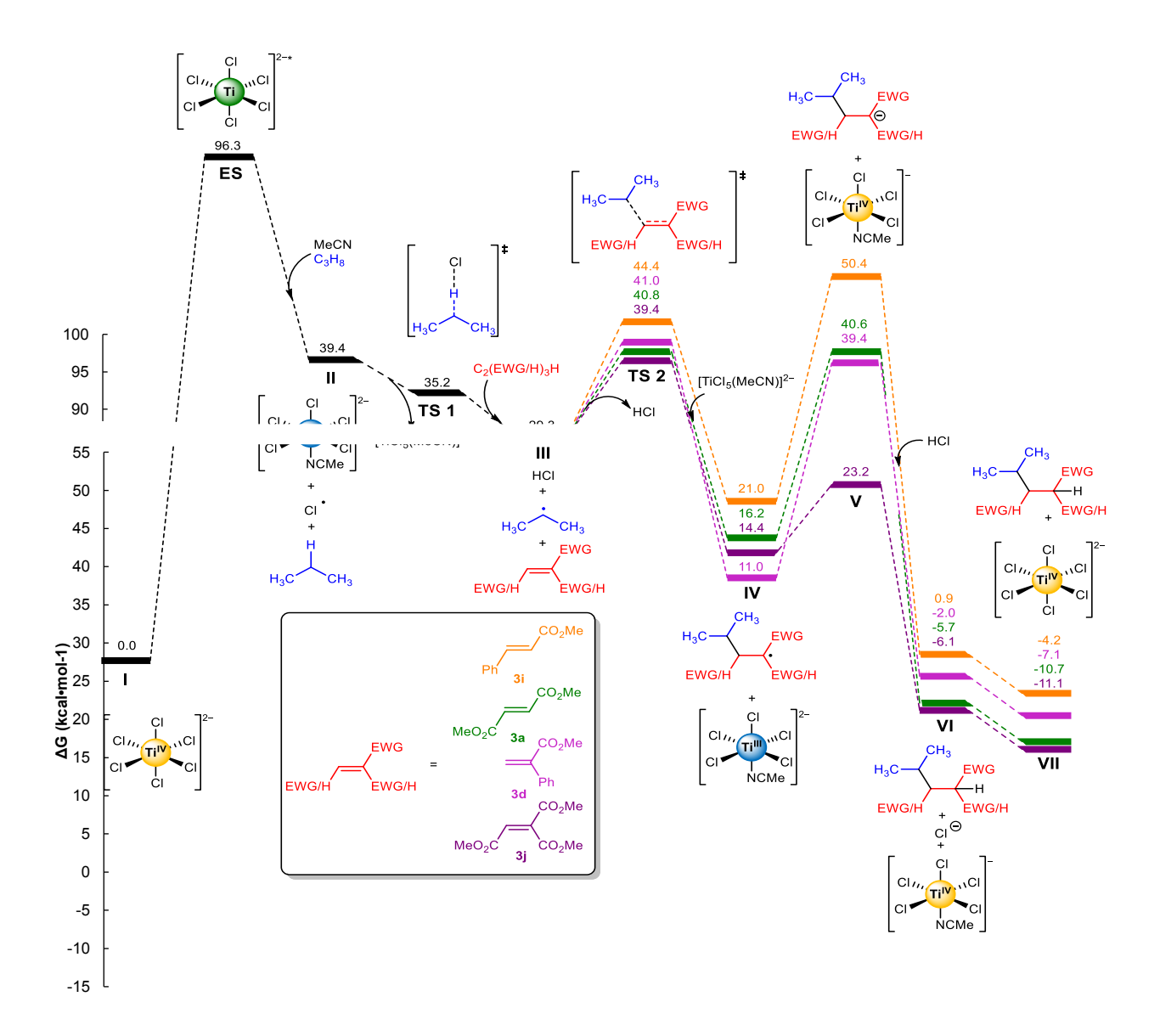


Figure 5. Energy profile of the catalytic reaction.
Radical traps: methyl cinnamate 3i, 3a, 3d, and trimethyl ethylenetricarboxylate 3j.

Discussion

We have demonstrated the ability of the earth abundant and inexpensive $TiCl_6{}^{2-}$ to activate the C–H bonds of unactivated hydrocarbons, including methane, under light irradiation. Photoexcitation into the LMCT band of $TiCl_6{}^{2-}$ results in the release of chlorine radical, which can activate the bonds of these hydrocarbon substrates. We found that where $CeCl_6{}^{2-}$ did not promote addition of radicals to alkenes that are only moderately electron poor, $TiCl_6{}^{2-}$ was successful, resulting in an increase in the scope of radical acceptors in this process. We determined that this broader scope was due to the more negative reduction potential of Ti^{III} species in solution, compared to the analogous Ce^{III} species under the same conditions. This observation was verified by electrochemical measurements and the isolation and detection of these species in the reaction media. Finally, the excited states and the reaction coordinate further establishes that the photoexcited state produces chlorine radical and that the reduction potential of the Ti^{III} species is integral to the formation of product and turnover of catalyst.

EXPERIMENTAL PROCEDURES

Standard catalytic procedures for condensed matter substrates.



In a N_2 filled glovebox, 0.2 mmol (1 equiv) of the unsaturated substrate was added to an 8 mL vial equipped with a Teflon coated stir bar. Subsequently, 4 mL of a 0.00125 M stock solution of 1 (0.025 equiv, 0.005 mmol, 5.3 mg) was added to the scintillation vial. Next, 0.6 mmol of alkane was added to the vial. The vial was capped and sealed with tape. The vial was removed from the glovebox and irradiated for 24 h using a Kessil PR160L-390 at 30 °C (provided by the heat of the lamp) with fan cooling. After irradiating, the reactions were exposed to air, quickly quenched by the addition of 4 drops of deionized water, and diluted with 4 mL of EtOAc. The mixture was passed through a silica plug and eluted using 3 x 2 mL of EtOAc. The volatile materials were removed using rotary evaporation and the resulting material subjected to silica gel column chromatography.

Resource Availability

Lead Contact

Further information and requests for resources and reagents should be directed to and will be fulfilled by the Lead Contact, Eric J. Schelter (schelter@sas.upenn.edu).

Materials Availability

All unique reagents generated in this study are available from the Lead Contact without restriction.

Data and Code Availability

Crystallographic data for the structures reported in this article have been deposited at the Cambridge Crystallographic Data Center (CCDC) under deposition nos. CCDC 2103224 (5a) and CCDC 2103225 (5b). These data can be obtained free of charge from the Cambridge Crystallographic Data Centre via www.ccdc.cam.ac.uk/data_request/cif. All other data supporting the findings of this study are available within the Article and its Supplemental Information and from the corresponding authors upon reasonable request.

SUPPLEMENTAL INFORMATION

Supplemental Information can be found online at https://doi.org/10.1016/j.chempr.xxxx.xx.xx

ACKNOWLEDGMENTS

E.J.S., P.J.W., and G.B.P. gratefully acknowledge the U.S. National Science Foundation (CHE-1955724 to E.J.S., CHE-1902509 to P.J.W., and Graduate Research Fellowship Program NSF-GRFP to G.B.P.) for primary support. This work used the Extreme Science and Engineering Discovery Environment (XSEDE), which is supported by the NSF (TG-CHE140012). We also thank the University of Pennsylvania and the Vagelos Institute for Energy Science and Technology at the University of Pennsylvania for support of this work.

AUTHOR CONTRIBUTIONS

G.B.P. and E.J.S. conceived this project. G.B.P. and Q.Y. performed the synthesis. G.B.P. performed the electrochemical, NMR, and UV-Vis experiments. M.R.G. and P.J.C. collected and solved the X-ray structures. G.B.P. performed the computational analysis. G.B.P., P.J.W., and E.J.S. analyzed the experimental data. G.B.P., Q.Y., P.J.W., and E.J.S. participated in drafting the paper. All authors discussed the results and contributed the preparation of the final manuscript.

DECLARATION OF INTERESTS

The authors declare no competing interests.

INCLUSION AND DIVERSITY

One or more of the authors of this paper self-identifies as a member of the LGBTQ+ community. One or more of the authors of this paper self-identifies as living with a disability.

REFERENCES

- 1. Ruscic, B. (2015). Active Thermochemical Tables: Sequential Bond Dissociation Enthalpies of Methane, Ethane, and Methanol and the Related Thermochemistry. J. Phys. Chem. A. 119, 7810-7837. 10.1021/acs.jpca.5b01346.
- 2. Olah, G.A., Gupta, B., Felberg, J.D., Ip, W.M., Husain, A., Karpeles, R., Lammertsma, K., Melhotra, A.K., and Trivedi, N.J. (1985). Electrophilic reactions at single bonds. 20. Selective monohalogenation of methane over supported acidic or platinum metal catalysts and hydrolysis of methyl halides over .gamma.-alumina-supported metal oxide/hydroxide



- catalysts. A feasible path for the oxidative conversion of methane into methyl alcohol/dimethyl ether. J. Am. Chem. Soc. 107, 7097-7105. 10.1021/ja00310a057.
- 3. Dumas, J. (1840). Ueber die Einwirkung des Chlors auf den aus essigsauren Salzen entstehenden Kohlenwasserstoff. Justus Liebigs Ann. Chem. 33, 187-189. 10.1002/jlac.18400330205.
- 4. Ohligschläger, A., Menzel, K., Ten Kate, A., Martinez, J.R., Frömbgen, C., Arts, J., McCulloch, A., Rossberg, M., Lendle, W., Pfleiderer, G., et al. (2021). Chloromethanes. In Ullmann's Encyclopedia of Industrial Chemistry, pp. 1-31. 10.1002/14356007.a06_233.pub4.
- 5. Schleede, A., and Luckow, C. (1922). Über die Chlorierung des Methans. Ber. dtsch. Che. Ges. A/B 55, 3710-3726. 10.1002/cber.19220551114.
- 6. Isse, A.A., Lin, C.Y., Coote, M.L., and Gennaro, A. (2011). Estimation of Standard Reduction Potentials of Halogen Atoms and Alkyl Halides. J. Phys. Chem. B. 115, 678-684. 10.1021/jp109613t.
- 7. Zhang, L., and Hu, X. (2017). Room temperature C(sp²)—H oxidative chlorination via photoredox catalysis. Chem. Sci. 8, 7009-7013. 10.1039/C7SC03010J.
- 8. Troian-Gautier, L., Turlington, M.D., Wehlin, S.A.M., Maurer, A.B., Brady, M.D., Swords, W.B., and Meyer, G.J. (2019). Halide Photoredox Chemistry. Chem. Rev. 119, 4628-4683. 10.1021/acs.chemrev.8b00732.
- 9. Zidan, M., Morris, A.O., McCallum, T., and Barriault, L. (2020). The Alkylation and Reduction of Heteroarenes with Alcohols Using Photoredox Catalyzed Hydrogen Atom Transfer via Chlorine Atom Generation. Eur. J. Org. Chem. 2020, 1453-1458. 10.1002/ejoc.201900786.
- 10. Bevernaegie, R., Wehlin, S.A.M., Piechota, E.J., Abraham, M., Philouze, C., Meyer, G.J., Elias, B., and Troian-Gautier, L. (2020). Improved Visible Light Absorption of Potent Iridium(III) Photo-oxidants for Excited-State Electron Transfer Chemistry. J. Am. Chem. Soc. 142, 2732-2737. 10.1021/jacs.9b12108.
- 11. Rohe, S., Morris, A.O., McCallum, T., and Barriault, L. (2018). Hydrogen Atom Transfer Reactions via Photoredox Catalyzed Chlorine Atom Generation. Angew. Chem. Int. Ed. 57, 15664-15669. 10.1002/anie.201810187.
- 12. Kariofillis, S.K., and Doyle, A.G. (2021). Synthetic and Mechanistic Implications of Chlorine Photoelimination in Nickel/Photoredox C(sp³)—H Cross-Coupling. Acc. Chem. Res. 10.1021/acs.accounts.0c00694.
- 13. Shields, B.J., and Doyle, A.G. (2016). Direct C(sp³)–H Cross Coupling Enabled by Catalytic Generation of Chlorine Radicals. J. Am. Chem. Soc. 138, 12719-12722. 10.1021/jacs.6b08397.
- 14. Treacy, S.M., and Rovis, T. (2021). Copper Catalyzed C(sp³)—H Bond Alkylation via Photoinduced Ligand-to-Metal Charge Transfer. J. Am. Chem. Soc. 143, 2729-2735. 10.1021/jacs.1c00687.
- 15. An, Q., Wang, Z., Chen, Y., Wang, X., Zhang, K., Pan, H., Liu, W., and Zuo, Z. (2020). Cerium-Catalyzed C–H Functionalizations of Alkanes Utilizing Alcohols as Hydrogen Atom Transfer Agents. J. Am. Chem. Soc. 142, 6216-6226. 10.1021/jacs.0c00212.
- 16. Hu, A., Guo, J.-J., Pan, H., and Zuo, Z. (2018). Selective functionalization of methane, ethane, and higher alkanes by cerium photocatalysis. Science 361, 668. 10.1126/science.aat9750.
- 17. Yang, Q., Wang, Y.-H., Qiao, Y., Gau, M., Carroll, P.J., Walsh, P.J., and Schelter, E.J. (2021). Photocatalytic C—H activation and the subtle role of chlorine radical complexation in reactivity. Science 372, 847. 10.1126/science.abd8408.
- 18. Kang, Y.C., Treacy, S.M., and Rovis, T. (2021). Iron-Catalyzed Photoinduced LMCT: A 1° C—H Abstraction Enables Skeletal Rearrangements and C(sp³)—H Alkylation. ACS Catal. 11, 7442-7449. 10.1021/acscatal.1c02285.
- 19. Jin, Y., Zhang, Q., Wang, L., Wang, X., Meng, C., and Duan, C. (2021). Convenient C(sp³)—H bond functionalisation of light alkanes and other compounds by iron photocatalysis. Green Chemistry 23, 6984-6989. 10.1039/D1GC01563J.
- 20. Jin, Y., Wang, L., Zhang, Q., Zhang, Y., Liao, Q., and Duan, C. (2021). Photo-induced direct alkynylation of methane and other light alkanes by iron catalysis. Green Chemistry 23, 9406-9411. 10.1039/D1GC03388C.
- 21. Zhu, Q., and Nocera, D.G. (2020). Photocatalytic Hydromethylation and Hydroalkylation of Olefins Enabled by Titanium Dioxide Mediated Decarboxylation. J. Am. Chem. Soc. 142, 17913-17918. 10.1021/jacs.0c08688.
- 22. Manley, D.W., McBurney, R.T., Miller, P., Howe, R.F., Rhydderch, S., and Walton, J.C. (2012). Unconventional Titania Photocatalysis: Direct Deployment of Carboxylic Acids in Alkylations and Annulations. J. Am. Chem. Soc. 134, 13580-13583. 10.1021/ja306168h.
- 23. Tsunoji, N., Nishida, H., Ide, Y., Komaguchi, K., Hayakawa, S., Yagenji, Y., Sadakane, M., and Sano, T. (2019). Photocatalytic Activation of C–H Bonds by Spatially Controlled Chlorine and Titanium on the Silicate Layer. ACS Catal. 9, 5742-5751. 10.1021/acscatal.9b01284.



- 24. Kunkely, H., and Vogler, A. (1998). Photoreactivity of Titanocene Pentasulfide. Z. Naturforsch. B 53, 224-226. doi:10.1515/znb-1998-0214.
- 25. Tehfe, M.-A., Lalevée, J., Morlet-Savary, F., Graff, B., and Fouassier, J.-P. (2012). On the Use of Bis(cyclopentadienyl)titanium(IV) Dichloride in Visible-Light-Induced Ring-Opening Photopolymerization. Macromolecules 45, 356-361. 10.1021/ma202307x.
- 26. Godemann, C., Dura, L., Hollmann, D., Grabow, K., Bentrup, U., Jiao, H., Schulz, A., Brückner, A., and Beweries, T. (2015). Highly selective visible light-induced Ti–O bond splitting in an ansa-titanocene dihydroxido complex. Chem. Commun. *51*, 3065-3068. 10.1039/C4CC09733E.
- 27. Zhang, Z., Hilche, T., Slak, D., Rietdijk, N.R., Oloyede, U.N., Flowers Ii, R.A., and Gansäuer, A. (2020). Titanocenes as Photoredox Catalysts Using Green-Light Irradiation. Angew. Chem. Int. Ed. *59*, 9355-9359. 10.1002/anie.202001508.
- 28. Morcillo, S.P., Miguel, D., Campaña, A.G., Álvarez de Cienfuegos, L., Justicia, J., and Cuerva, J.M. (2014). Recent applications of Cp₂TiCl in natural product synthesis. Org. Chem. Front. 1, 15-33. 10.1039/C3QO00024A.
- 29. Minasian, S.G., Keith, J.M., Batista, E.R., Boland, K.S., Clark, D.L., Conradson, S.D., Kozimor, S.A., Martin, R.L., Schwarz, D.E., Shuh, D.K., et al. (2012). Determining Relative f and d Orbital Contributions to M–Cl Covalency in MCls²⁻ (M = Ti, Zr, Hf, U) and UOCls⁻ Using Cl K-Edge X-ray Absorption Spectroscopy and Time-Dependent Density Functional Theory. J. Am. Chem. Soc. 134, 5586-5597. 10.1021/ja2105015.
- 30. Yin, H., Jin, Y., Hertzog, J.E., Mullane, K.C., Carroll, P.J., Manor, B.C., Anna, J.M., and Schelter, E.J. (2016). The Hexachlorocerate(III) Anion: A Potent, Benchtop Stable, and Readily Available Ultraviolet A Photosensitizer for Aryl Chlorides. J. Am. Chem. Soc. 138, 16266-16273. 10.1021/jacs.6b05712.
- 31. Wu, Y.-D., Wong, C.-L., Chan, K.W.K., Ji, G.-Z., and Jiang, X.-K. (1996). Substituent Effects on the C-H Bond Dissociation Energy of Toluene. A Density Functional Study. J. Org. Chem. 61, 746-750. 10.1021/jo951212v.
- 32. Tian, Z., Fattahi, A., Lis, L., and Kass, S.R. (2006). Cycloalkane and Cycloalkene C–H Bond Dissociation Energies. J. Am. Chem. Soc. 128, 17087-17092. 10.1021/ja065348u.
- 33. Tsurkan, M.V., Jungnickel, C., Schlierf, M., and Werner, C. (2017). Forbidden Chemistry: Two-Photon Pathway in [2+2] Cycloaddition of Maleimides. J. Am. Chem. Soc. 139, 10184-10187. 10.1021/jacs.7b04484.
- 34. Jones, N.A., Liddle, S.T., Wilson, C., and Arnold, P.L. (2007). Titanium(III) Alkoxy-N-heterocyclic Carbenes and a Safe, Low-Cost Route to TiCl3(THF)3. Organometallics 26, 755-757. 10.1021/om060486d.
- 35. Chen, L., and Cotton, F.A. (1998). Synthesis, reactivity, and X-ray structures of face-sharing Ti(III) complexes; the new trinuclear ion, $[Ti_3Cl_{12}]^{3-}$. Polyhedron 17, 3727-3734. 10.1016/S0277-5387(98)00171-5.
- 36. Castro, S.L., Streib, W.E., Huffmann, J.C., and Christou, G. (1996). A mixed-valence (TiTi) carboxylate complex: crystal structures and properties of [Ti₂OCl₃(O₂CPh)₂(thf)₃] and [NEt₄]₃[Ti₂Cl₉]. Chem. Commun., 2177-2178. 10.1039/CC9960002177.
- 37. Zhao, Y., and Truhlar, D.G. (2008). The M06 suite of density functionals for main group thermochemistry, thermochemical kinetics, noncovalent interactions, excited states, and transition elements: two new functionals and systematic testing of four M06-class functionals and 12 other functionals. Theor. Chem. Account 120, 215-241. 10.1007/s00214-007-0310-
- 38. Dunning, T.H. (1989). Gaussian basis sets for use in correlated molecular calculations. I. The atoms boron through neon and hydrogen. J. Chem. Phys. 90, 1007-1023. 10.1063/1.456153.
- 39. Zhang, J.-P., Wang, Y., Ma, J.-B., Jin, L., Liu, F.-T., and Bai, F.-Q. (2018). Density functional theory investigation on iridium(iii) complexes for efficient blue electrophosphorescence. RSC Adv. 8, 19437-19448. 10.1039/C8RA02858C.